

# Appearance of caustics in dynamic spectra

Artem Tuntsov for the ATESE Team – 2017/05/04

A curious radio spectrum of the source PMN J1106-3647 obtained on MJD 57087 in the course of the Australia Telescope survey for Extreme Scattering Events (ATESE, Bannister et al. 2016) displayed a sharp kink (Figure 8) that was difficult to explain in a conventional way (Tuntsov et al., 2017). Instead, we suspected it was associated with a caustic crossing, with the source seen on the opposite sides of the caustic at different frequencies due to wavelength dependence of its position. This prompted the present study of the qualitative appearance and behaviour of the caustic in the dynamic spectrum, which helps understand the evolution of caustic features in the spectra. One other potential application is spectra of Fast Radio Bursts (FRBs) which might be disproportionately affected by lensing in the plasma of their hosts or intervening galaxies – indeed, lensing can be responsible for at least some of their unusual properties (Cordes et al., 2017). We hope that this study might inform future analyses of the phenomenology of the spectral features caused by caustics in plasma lensing.

The first part studies the morphology of the caustics and the relationship between the behaviour of the plasma column density (via its derivative) and the caustic. The second part considers the behaviour of the observable, the flux density, near to and through the caustic crossing; some of the qualitative features of light curves or instantaneous spectra might be used to infer the shape of the source – in particular, a kink of the shape seen in the data, suggest a *concave* source. The treatment is refractive (i.e., ray optics) throughout, we limit ourselves to the one-dimensional case, appropriate not only for the highly anisotropic plasma but in general for the most common type of singularity, a fold; the style is informal at places. It is our intention to publish the analysis of the 2D case, which has a much richer phenomenology due to the presence of two principal directions, further along the way.

## 1 Caustic shapes in 1D case

In the geometric optics approximation, the plasma lens equation maps the position  $\theta$  of a ray in the lens (image) plane to its origin  $\beta$  in the source plane:

$$\beta(\theta, \lambda) = \theta - \lambda^2 \alpha(\theta) \quad (1)$$

where  $\lambda$  is the wavelength of radiation and  $\alpha$  is the deflection angle at unit wavelength.

A caustic forms where the mapping (1) becomes singular

$$\frac{\partial \beta}{\partial \theta} = 0 \Rightarrow 0 = 1 - \lambda^2 \alpha'(\theta), \quad (2)$$

where the prime denotes differentiation with respect to  $\theta$ . As  $\lambda^2 \geq 0$ , the equation only has solution if  $\alpha' \geq 0$ , in which case the caustic forms at the sufficiently long wavelength

$$\lambda(\theta) = \frac{1}{\sqrt{\alpha'(\theta)}}, \quad \alpha'(\theta) > 0, \quad (3)$$

which in turn defines the position of the point on the caustic curve in the source plane

$$\beta(\theta) = \theta - \frac{\alpha(\theta)}{\alpha'(\theta)} \quad (4)$$

Together equations (3, 4) parametrically define the caustic curve in the  $(\beta, \lambda)$  plane, which maps directly onto the dynamic spectrum via an inversion of  $\lambda$  and a kinematical model  $t \rightarrow \beta$ . For convenience, we will use  $u \equiv \lambda^2$  instead of the frequency; this simplifies subsequent formulae.

We are thus left with an analysis exercise of studying a parametrically defined curve  $(u(\theta), \beta(\theta))$  corresponding to a given deflection curve  $\alpha(\theta)$  when  $\alpha'(\theta)$  is positive. As  $\alpha'(\theta)$  increases from zero at some  $\theta_0$ , the caustic comes down along an oblique asymptote

$$\beta(u) \xrightarrow{u \rightarrow \infty} \beta_0(u) = \theta_0 - \alpha(\theta_0)u \quad (5)$$

until  $\alpha'$  reaches a maximum at some  $\theta_1$ . At the turning point,

$$u_1 = \frac{1}{\alpha'(\theta_1)}, \quad \beta_1 = \theta_1 - \frac{\alpha(\theta_1)}{\alpha'(\theta_1)} \quad (6)$$

the curve must bounce off and head back up, as  $\alpha'(\theta) < \alpha'(\theta_1)$  near the local maximum. It does so in a very specific way, by forming a cusp (this cusp is not to be confused with the cusps forming in 2D lensing – *e.g.*, those discussed in Section 2.2.2). That is because the caustic curve never runs level (on the  $u$  vs  $\beta$  plot); it is an envelope curve of the characteristic system<sup>1</sup> (as new images are formed on crossing it) and therefore tangential to characteristics, which are never parallel to the  $\beta$  axis. Indeed,

$$\dot{\beta} = \frac{d\beta}{du} = \frac{\partial \beta}{\partial \theta u} = \frac{1 - 1 + \alpha \alpha'' / (\alpha')^2}{-\alpha'' / (\alpha')^2} = -\alpha. \quad (7)$$

<sup>1</sup>Following Tuntsov et al. (2015) we call the line  $(\beta, \lambda)$  defined by setting  $\theta = \text{const}$  in (1) a characteristic.

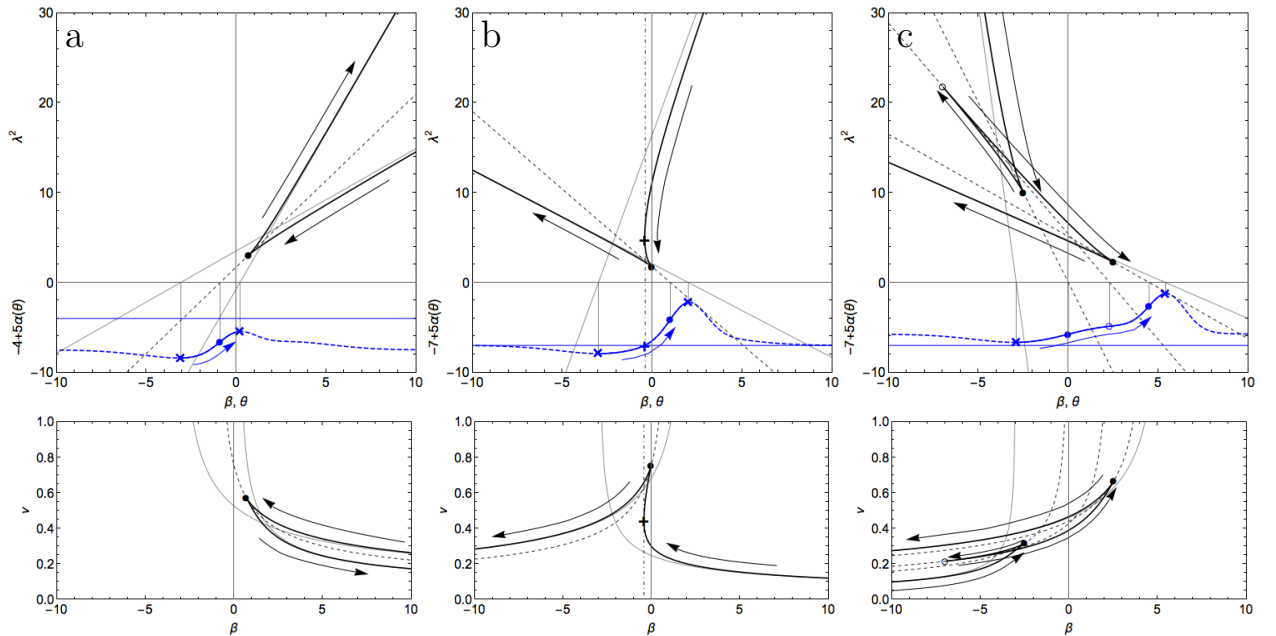


Figure 1: Possible shapes of caustics in the one-dimensional case: (a) a simple caustic with a single cusp, (b) a simple caustic that bends back and (c) a complex caustic with one primary and a pair of secondary cusps. The thick black curves are the caustics that correspond to the deflection curve  $\alpha(\theta)$  shown in blue; zero deflection level is shown as a blue horizontal line. The top panels show squared wavelength  $vs$  source position plots and on the bottom are frequency  $vs$  source position plots, more similar to the standard representation of the dynamic spectra. The crosses are the endpoints of the  $\alpha'(\theta) > 0$  intervals, the circles are stationary points of  $\alpha'$  (filled for local maxima and open for local minima) and the plus sign marks the root of the deflection curve,  $\alpha(\theta) = 0$ . Thin black lines show the asymptotes defined by the endpoints (solid), midlines of cusps (dashed) and tangents to caustics at bend-back points (dot-dashed); these are straight lines. The black arrows indicate the path of the caustic point that corresponds to the point following the deflection line as marked by the blue arrow.

Therefore, as a point follows the caustic curve near the turning point, it has to stop and turn back – *i.e.*, go through a cusp. Meanwhile the sign of the curvature (w.r. to the  $u$  axis) of the caustic curve reverses,

$$\ddot{\beta} = \frac{d\dot{\beta}}{du} = \frac{-\alpha'}{-\alpha''/(\alpha')^2} = \frac{(\alpha')^3}{\alpha''}, \quad (8)$$

as the values of  $\alpha''$  on the two sides of a local maximum of  $\alpha'$  are of opposite signs. The reversal implies that the two branches of the caustic curve that join at the turn-off point diverge onto the opposite sides of their common tangent line. Figure 1a presents an example of such a caustic.

Where this common tangent is not vertical,  $\alpha \neq 0$ , the divergence in turn implies that the  $u(\beta)$  function becomes multi-valued. Since the inside of a caustic has additional images, which are generally magnified, this would normally lead to the presence, in a single spectrum ( $\beta = \text{const}$ ) of a finite segment of some enhanced flux density. If the deflection angle passes through zero at a non-stationary point of  $\alpha'$  the caustic curve continues smoothly and bends back in  $\beta$  without forming a cusp, remaining on the same side of its vertical tangent, as shown in Figure 1b. In this case  $u(\beta)$  becomes multi-valued, too, but the phenomenology of a spectrum dissecting such bend would be of opposite nature, containing, generally, a finite segment of diminished flux density.

The reasoning of the paragraph describing the cusp can be applied, without modification, to local minima of  $\alpha'(\theta)$ , which implies that the turn-off from an increasing to decreasing  $u$  must also happen via formation of a cusp. However, unlike a maximum, a minimum has not be present, as  $\alpha'$  may increase from zero to a positive value and return to zero without passing through a local minimum. If a local minimum is present, there has to be an additional local maximum since  $\alpha'$  must return to zero. Therefore, there is always one more cusp pointing down than there are those pointing up. Figure 1c presents an example of such complex caustic and figure 2c shows an example of spectra this caustics can cause.

Given these properties we can sketch the caustic curve – or, rather, caustic curves – as images of those sections of the deflection curve where the deflection angle is monotonically increasing. If those monotonicity intervals are finite (which is probably the case for all realistic deflection curves with a finite range of the deflection angle), each caustic curve consists of two branches emerging from a cusp pointing down and asymptoting to oblique lines (5). The intercept and slope of each asymptote are given by substituting  $\theta_0$  with the interval end points while the cusp is located at (6) with  $\theta_1$  replaced by the position where  $\alpha'(\theta)$  attains its maximum and tilted as per the value of the deflection angle at this position. Additional pairs of cusps – one pointing up, the other down – might be present on any branch of the caustic curve if the monotonicity interval contains local minima of  $\alpha'$ . As  $\alpha$  is monotonic on the interval, the orientation of the tangent line to the caustic changes in a consistent direction (counter-clockwise on the  $u$  vs  $\beta$  plot as the curve is followed in the order of increasing  $\theta$ ) along the caustic curve, between the extremes given by the two

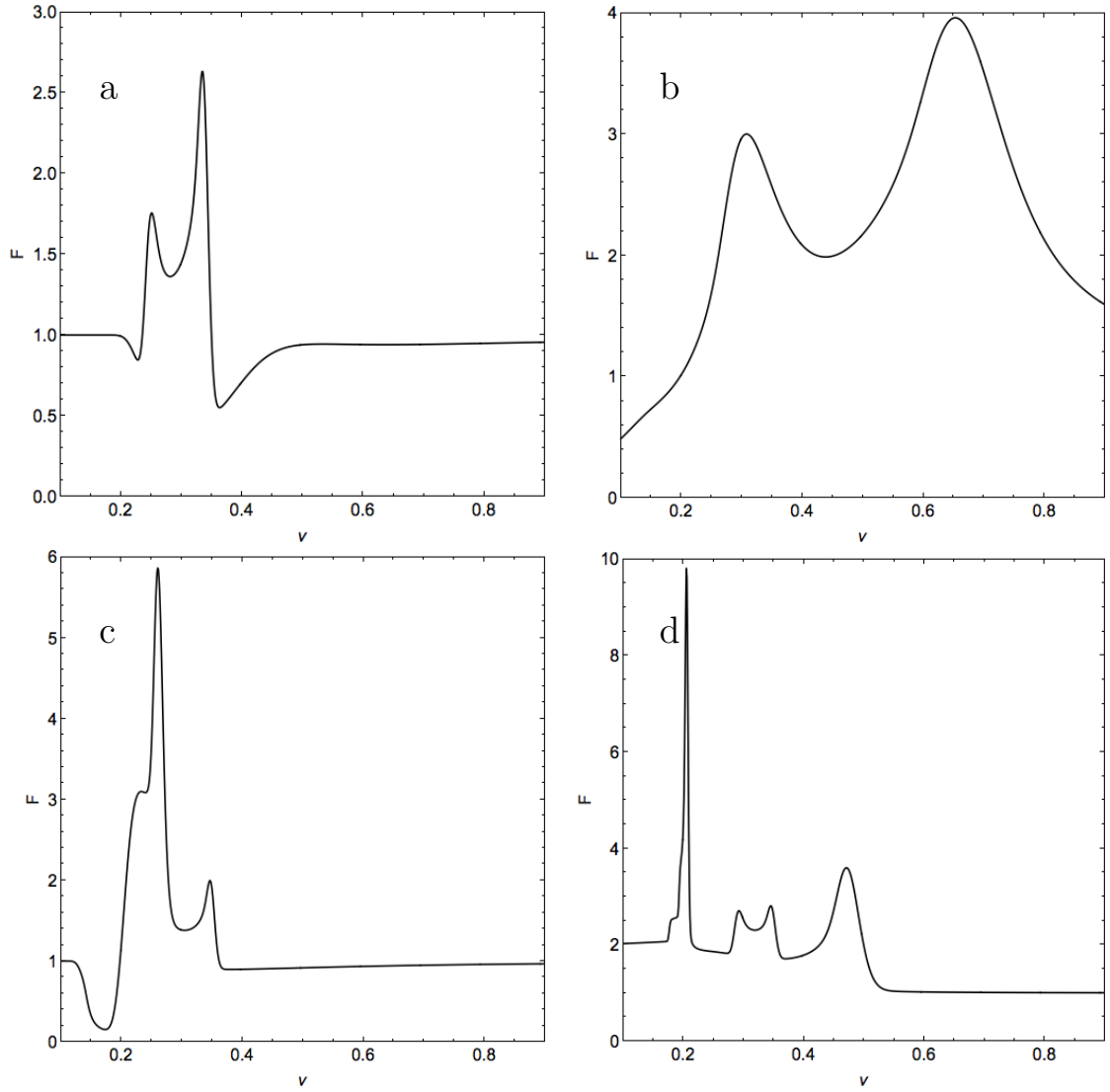


Figure 2: Examples of individual spectra produced by deflection curves shown at Figure 1 (a-c, respectively, with spectra plotted for  $\beta$  values of 5,  $-0.3$  and  $-4$ , respectively. Panel d shows the spectrum produced by the deflection curve in Figure 3 cut at  $\beta = -4$ . In all cases a Gaussian source of unit flux density with size  $\sigma = 0.3$  is assumed.

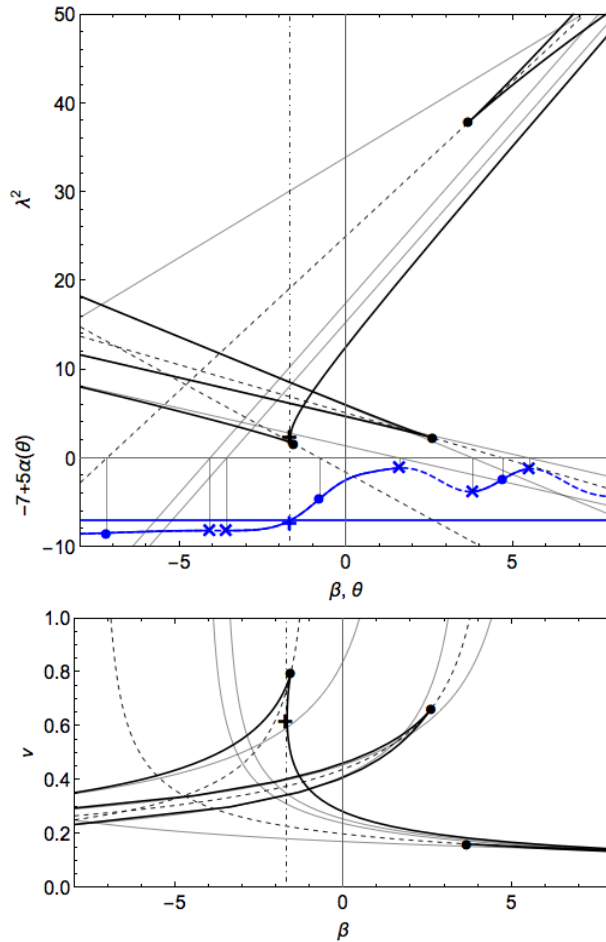


Figure 3: Possible layout of separate caustics in the one-dimensional case; the mark-up is the same as in Figure 1. The deflection curve shown has three intervals of increasing  $\alpha(\theta)$ , to which three separate caustics correspond. The insides of caustics intersect resulting in a complex behaviour of multiplicity and flux density across the plot.

asymptotes. Finally, another possible point of interest is where the deflection angle vanishes, which marks the position at which the caustic curve bends back in  $\beta$  smoothly (assuming  $\alpha'' \neq 0$ ); only one such point might be present on each caustic curve due to monotonicity of  $\alpha$ .

Inside each caustic curve the source is multiply imaged and there seem to be few restrictions on the relative placement of separate caustic curves corresponding to distinct intervals of monotonic increase in the deflection angle – essentially because the deflection curve is free to behave in whatever fashion in the intervening segments of non-increasing  $\alpha$ . Therefore, separate caustic curves might intersect each other implying potentially very complex behaviour of the image multiplicity as a function of position in the dynamic spectrum (or the  $u$  vs  $\beta$  plot). An example of possible arrangement of three caustics along with the deflection curve that generates them is shown in Figure 3; corresponding spectrum is shown in Figure 2c. One restriction is that, since the deflection angle is not increasing in the intervening sections, the direction of the right asymptote of each curve should be no ‘earlier’ (in the clock analogy) than that of the left asymptote of the preceding curve. However, this direction can change arbitrarily (or nearly so, as the tangent line cannot be horizontal) along each curve, and therefore the restriction applies to two successive curves only. It is nevertheless possible to infer the actual order of curves through considering the intervals formed by the intercept of the asymptotes on the  $\beta$  axis (as intercepts are precisely the endpoints of monotonicity intervals) but it remains to be seen if this information is sufficient to test the restriction in practice, when the coverage of the dynamic spectrum is necessarily limited in both time and frequency. Likewise, there do not seem to be reasons why a caustic curve cannot intersect itself if it contains pairs of extra cusps, where a point following the curve turns around (indeed, the curve in Figure 1b does intersect itself); self-intersection is not possible for simple caustic curves (containing a single cusp).

Most of the results above were formulated for a plot showing the squared wavelength versus the source position, which relates to the deflection curve in a linear way via (1). This provides a simple geometrical interpretation for many of the properties discussed (in particular, characteristics become their own tangents), which one might expect contribute to developing some intuition about the properties of the caustic curves. However, they carry over straightforwardly to the usual representation of the dynamic spectrum as a function of time and frequency, since the former is supposed to be a linear function of the position in the source plane (assuming uniform rectilinear motion with negligible parallax) and the latter is just the inverse square root of the squared wavelength. Thus, in effect, only one of the coordinate is affected in a non-trivial way and although non-linear, this latter transformation is regular for all frequencies of interest. Therefore, inferences based on the first derivatives are unaffected; in particular, cusps remain cusps. However, the second derivative attains an extra term containing the second derivative of the  $\lambda^2 \rightarrow \nu$  transform, which affects the relationship between the curvatures of caustic branches; they still diverge onto the different sides

of the cusp mid-line but the latter is no longer a straight line. The other inconvenience is that the asymptotes (5) become a bit more complicated,

$$\beta_0(\nu) = \theta_0 - \frac{\alpha(\theta_0)}{\nu^2} \quad \text{or} \quad \nu_0(\beta) = \sqrt{\frac{\alpha(\theta_0)}{\theta_0 - \beta}}, \quad (9)$$

and one has to mentally follow such characteristics to infinity in  $\nu$  rather than straight lines to  $\lambda^2 = 0$  when eye-balling their respective  $\theta_0$  values.

## 2 Behaviour of flux density near a caustic

In the geometric optics, the surface brightness is conserved even as a caustic is approached. Therefore, the enhancement of the flux density is given by the size ratio of the image(s) and the source. The linear term in the Taylor expansion of the mapping (1) between the two<sup>2</sup>:

$$\beta_0 + \Delta\beta = \theta_0 + \Delta\theta - \lambda^2\alpha(\theta_0) - \lambda^2\alpha'(\theta_0)\Delta\theta - \frac{\lambda^2}{2!}\alpha''(\theta_0)\Delta\theta^2 + \mathcal{O}(\Delta\theta^3) \quad (10)$$

vanishes at the caustic, according to (2) and the quadratic term becomes dominant:

$$\Delta\beta \simeq -\frac{\lambda^2}{2!}\alpha''(\theta_0)\Delta\theta^2 = -\text{sgn}\alpha''(\theta_0)\frac{\lambda^2}{2}\left(\frac{\Delta\theta}{\rho}\right)^2 \rho, \quad (11)$$

where the characteristic scale of the caustic has been introduced:

$$\rho \equiv \frac{1}{|\alpha''(\theta_0)|} \quad (12)$$

There are two solutions to (11) formed either side of the critical curve (the image of the caustic curve under (1)):

$$\Delta\theta = \pm \frac{1}{\lambda} \sqrt{-\frac{2\Delta\beta}{\alpha''(\theta_0)}} \quad (13)$$

which only appear when the source is on one side of the caustic,  $\text{sgn}\Delta\beta = -\text{sgn}\alpha''_0$ . For an infinitesimal source, the magnification of each image is given by the derivative

$$\mu = \frac{d\Delta\theta}{d\Delta\beta} = \mp \frac{1}{\lambda} \sqrt{\frac{\rho}{2\Delta\beta}}, \quad (14)$$

which diverges as  $\Delta\beta \rightarrow 0$ . The image present when the source is on the other side of the caustic is not generally much affected by crossing it, hence the behaviour of the total flux near the crossing is dominated by the pair (13).

### 2.1 Light curves of finite size sources

For a finite source (and the unbound magnification at the caustic resolves any source) with the intensity density  $I(\beta - \beta_c)$ , with some nominal centre  $\beta_c$  (introduced for the ease of intuitive interpretation), the flux density in the pair of images straddling the critical line is given by the integral over the part of the source that has crossed inside the caustic:

$$F(\beta_0 - \beta_c) = 2 \int_0^\infty d\zeta I\left(\beta_0 - \beta_c - \frac{\lambda^2}{2}\alpha''\zeta^2\right) = 2 \int_0^\infty \frac{d\xi I(\beta_0 - \beta_c - \text{sgn}\alpha''_0\xi)}{\lambda\sqrt{2\xi/\rho}} \quad (15)$$

where the factor in front of the integral is due to there being two images (13), which are identical to this accuracy. The first integral simply expresses the conservation of surface brightness, but the alternative, expressing the total flux density as an average of the magnification, is often better suited for practical applications. It is clear that a sufficiently compact source would brighten gradually once its leading side hits the caustic, peak shortly after it is fully inside and fade approximately as  $\Delta\beta^{-1/2}$  when its trailing side is well past it but the singularity at  $\xi \rightarrow 0$  is mild enough that the integral is not necessarily dominated by the source structure near it.

Closed form expressions can be obtained for many models of the source structure. For a Gaussian of flux density  $F_0$  and size  $\sigma$  centred at  $\beta_c$  it is

$$F_G(\beta_c - \beta_0) = \frac{F_0}{\lambda\sqrt{\sigma/\rho}} f_G\left(\frac{\beta_c - \beta_0}{\sigma}\right) \quad (16)$$

$$f_G(x) \equiv \frac{\sqrt{\pi|x|}}{2} e^{-x^2/4} \begin{cases} I_{-1/4}(x^2/4) + I_{1/4}(x^2/4), & x \leq 0 (\beta_c \text{ is inside the caustic}) \\ \frac{\sqrt{2}}{\pi} K_{1/4}(x^2/4), & x \geq 0 (\beta_c \text{ is outside}) \end{cases} \quad (17)$$

<sup>2</sup>There is some discontinuity in notation here from the previous section as  $\beta_0$ ,  $\theta_0$  now mark the positions of the caustic and critical curve at a given  $\lambda$  rather than particular points of the caustic itself. However, adding an extra subscripts to all  $\beta$  and  $\theta$  of the previous section would have made the notation unwieldy.

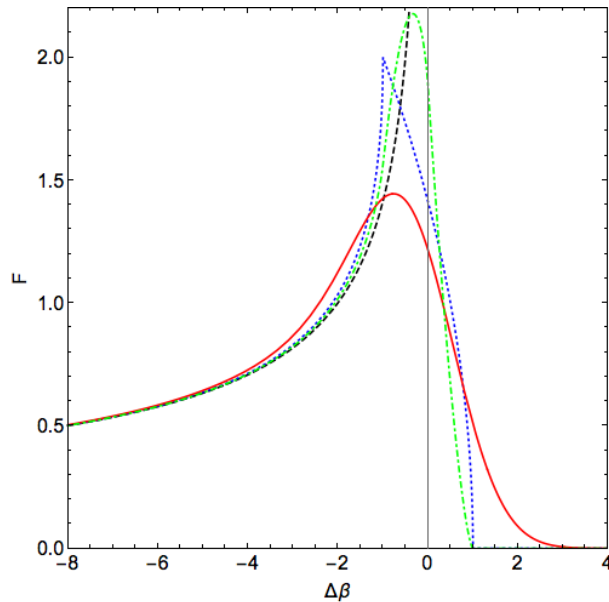


Figure 4: Flux density in the pair of images of a point-like (dashed, black), top hat (dotted, blue),  $\Lambda$  hat (dot-dashed, green) and Gaussian (solid, red) sources of unit intrinsic flux density that appear near the critical curve as the source enters inside the caustic. The horizontal axis is the distance from the caustic to the centre of the source in units of source size  $\sigma$  (or an arbitrary unit for the point-like source); the centre is inside the caustic at  $\Delta\beta < 0$  and outside it for  $\Delta\beta > 0$ . The unit of flux density depends on the caustic scale  $\rho$  and is given by the square root of its value in the horizontal scale units.

where  $I_{\pm 1/4}$  and  $K_{1/4}$  are modified Bessel functions of the first and second kind, respectively. This function reaches a maximum of

$$f_G \approx 1.4441 \quad \text{at} \quad x \approx -0.76495. \quad (18)$$

For a top hat source with the same parameters ( $\sigma$  being half-width) the result is elementary:

$$F_T(\beta_c - \beta_0) = \frac{F_0}{\lambda\sqrt{\sigma/\rho}} f_T\left(\frac{\beta_c - \beta_0}{\sigma}\right)$$

$$f_T(x) \equiv \sqrt{2} \begin{cases} \sqrt{-x+1} - \sqrt{-x-1}, & x \leq -1 \text{ (fully inside)} \\ \sqrt{-x+1}, & -1 \leq x \leq 1 \text{ (partly inside)} \\ 0, & x \geq 1 \text{ (fully outside)} \end{cases} = \sqrt{2} \operatorname{Re}(\sqrt{-x+1} - \sqrt{-x-1}) \quad (19)$$

note that all alternatives can be represented by taking the real part of the top line. Flux density of a top hat source peaks just as it gets fully into the caustic inside:

$$f_T(1) = 2. \quad (20)$$

As the intensity density is discontinuous at the edge of a top hat source, the flux density is not only non-smooth across the caustic but its derivative diverges. A  $\Lambda$  hat (rising linearly from the edge to the centre) is some halfway between a top hat and a Gaussian in terms of the smoothness of its transition to zero; its flux density near a caustic is given by

$$F(\nu) = \frac{F_0}{\lambda\sqrt{\sigma/\rho}} f_\Lambda\left(\frac{\beta_c - \beta_0}{\sigma}\right), \quad f_\Lambda(x) \equiv \frac{4\sqrt{2}}{3} \operatorname{Re}\left[(-x+1)^{3/2} - 2(-x)^{3/2} + (-x-1)^{3/2}\right]; \quad (21)$$

Its maximum is

$$f_\Lambda\left(\frac{1}{3}\right) = \frac{8\sqrt{2}}{3\sqrt{3}} \quad (22)$$

Figure 4 shows the behaviour of flux density in the two extra images for a point-like, Gaussian, top and  $\Lambda$  hat sources.

## 2.2 Explaining kinks

A top hat is not a particularly natural model for a source crossing a fold caustic because in the actual two dimensions it corresponds to a *rectangular* source with its side parallel to the caustic; the  $\Lambda$  hat similarly models the less restrictive case of a general orientation of the source, in which case it is the rectangle's angle that first appears on the caustic and the rest of the source follows<sup>3</sup>. More generally, a convex source with a smooth boundary first touches the fold

<sup>3</sup>The Gaussian model is not unnatural though as the projection of a 2D Gaussian onto an axis is also a Gaussian.

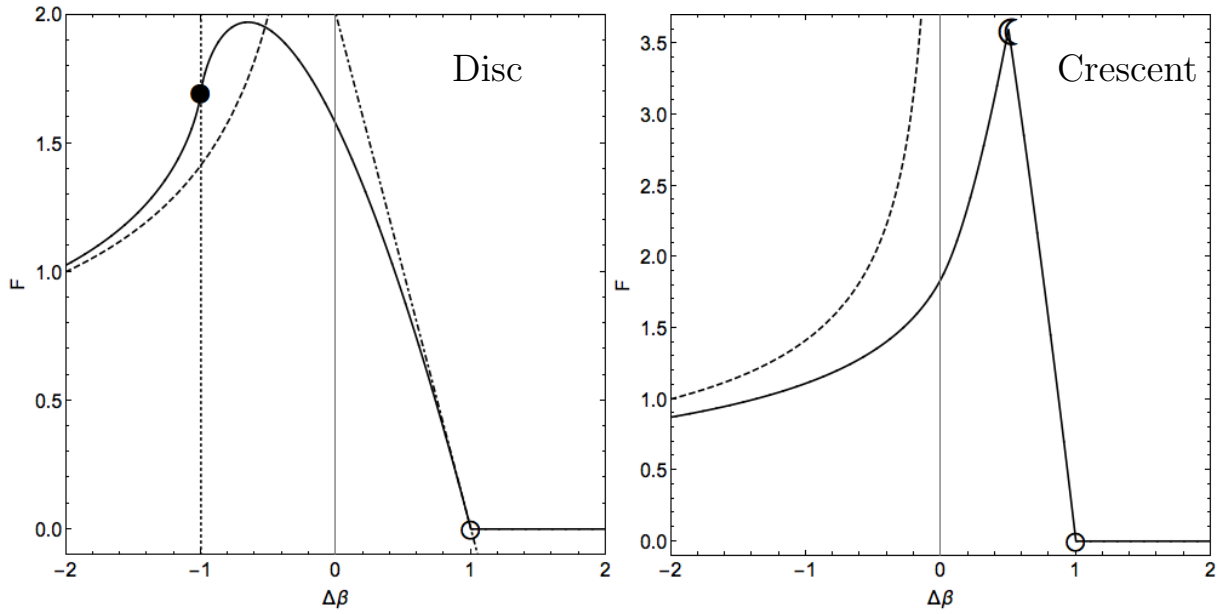


Figure 5: *Left.* Flux density in the pair of images of a circular disc source of unit intrinsic flux density and the point-like approximation (dashed line). The empty and filled circles mark the positions of the initial and final contacts with the caustic, respectively, and the dot-dashed line is the approximation (24). *Right.* Flux density in the extra images of a crescent source of unit flux density with an elliptic terminator and maximum width of half the radius. The circle marks the position of the caustic contact with the limb and the terminator, respectively.

caustic at a single point and the length of the intersection between the caustic and the source increases as a square root of the depth  $\delta\beta$  that the caustic has reached into the source:

$$l(\delta\beta) \simeq 2\sqrt{2\delta\beta B}, \quad (23)$$

where  $B$  is the source boundary curvature radius at the contact point. Thus, for a source of constant intensity density  $F_0/A$ ,  $A$  being the source's area, the flux density near the ingress is

$$F_i(\delta\beta) = \frac{F_0\sqrt{2\rho}}{\lambda A} \int_0^{\delta\beta} \frac{d\xi l(\delta\beta - \xi)}{\sqrt{\xi}} \simeq \frac{2\pi F_0\sqrt{B\rho}}{\lambda A} \delta\beta, \quad (24)$$

– *i.e.*, a linear function, which has a constant derivative. Before the crossing,  $\delta\beta < 0$ , this derivative is zero, as the two extra images have not appeared yet; in other words, at the first contact, on the start of the ingress, we have a sharp angle between two adjacent linear segments of the light curve. This might seem like what is needed to explain the remarkable kinks observed in the instantaneous spectra of some sources undergoing lensing events discovered in the ATESE survey (as explained in Section A the instantaneous spectrum crossing a caustic line in the dynamic spectrum at a generic point is essentially – up to a linear transform – the light curve of the source traversing the caustic on the sky).

However, the kinks in the instantaneous spectra are seen at local maxima, whereas at the start of the ingress a local minimum is achieved; it does not seem possible to turn one into another with the transformations used to turn, near the caustic, the light curve into an instantaneous spectrum (basically, rescaling the horizontal axis and adding a linear function). The final contact, the end of the egress for such source is not helping either as the two situations are not symmetric because of the asymmetry on the two sides of the caustic. The flux density of a (convex, smoothly bounded, constant intensity density) source that is  $\delta\beta$  before from the final contact is

$$F_e(\delta\beta) = \frac{F_0\sqrt{2\rho}}{\lambda A} \int_0^{\delta\beta} \frac{d\xi l(\delta\beta + \xi)}{\sqrt{\xi}} \simeq \frac{4F_0\sqrt{B\rho}}{\lambda A} \left[ -\frac{\delta\beta}{2} \log|\delta\beta| + \delta\beta \log\left(\sqrt{b} + \sqrt{b - \delta\beta}\right) + \sqrt{b(b - \delta\beta)} + f_{\text{other}}(\delta\beta) \right] \quad (25)$$

where  $f_{\text{other}}(\delta\beta)$  is a slowly varying contribution of the source region outside the applicability limit  $b$  of (23), which, along with the second and third terms in the square brackets, is well-behaved at  $\delta\beta \rightarrow 0$ . The derivative of the first term, on the contrary, diverges, logarithmically, at the final contact but the light curve continues smoothly beyond the final contact zone despite the divergence of the derivative on the other side of the vertical tangent at  $\delta\beta = 0$  – indeed, expression (25) remains valid into  $\delta\beta < 0$ . Hence, instead of a kink at a maximum we get more like a cliff face – a weak, logarithmic one. And at least for a symmetric source, it will be superposed on a declining light curve, since the flux density derivative should have crossed zero before the egress finishes because the  $1/\sqrt{\xi}$  factor biases its integral towards negative  $l'(\delta\beta - \xi)$  found past the source symmetry line. Figure 5 illustrates these points for a disc of constant surface brightness.

The question is then what sources *can* produce the kink at a local maximum. The preceding argument appears general enough to suggest this is not possible for a convex source of constant surface brightness with a smooth boundary

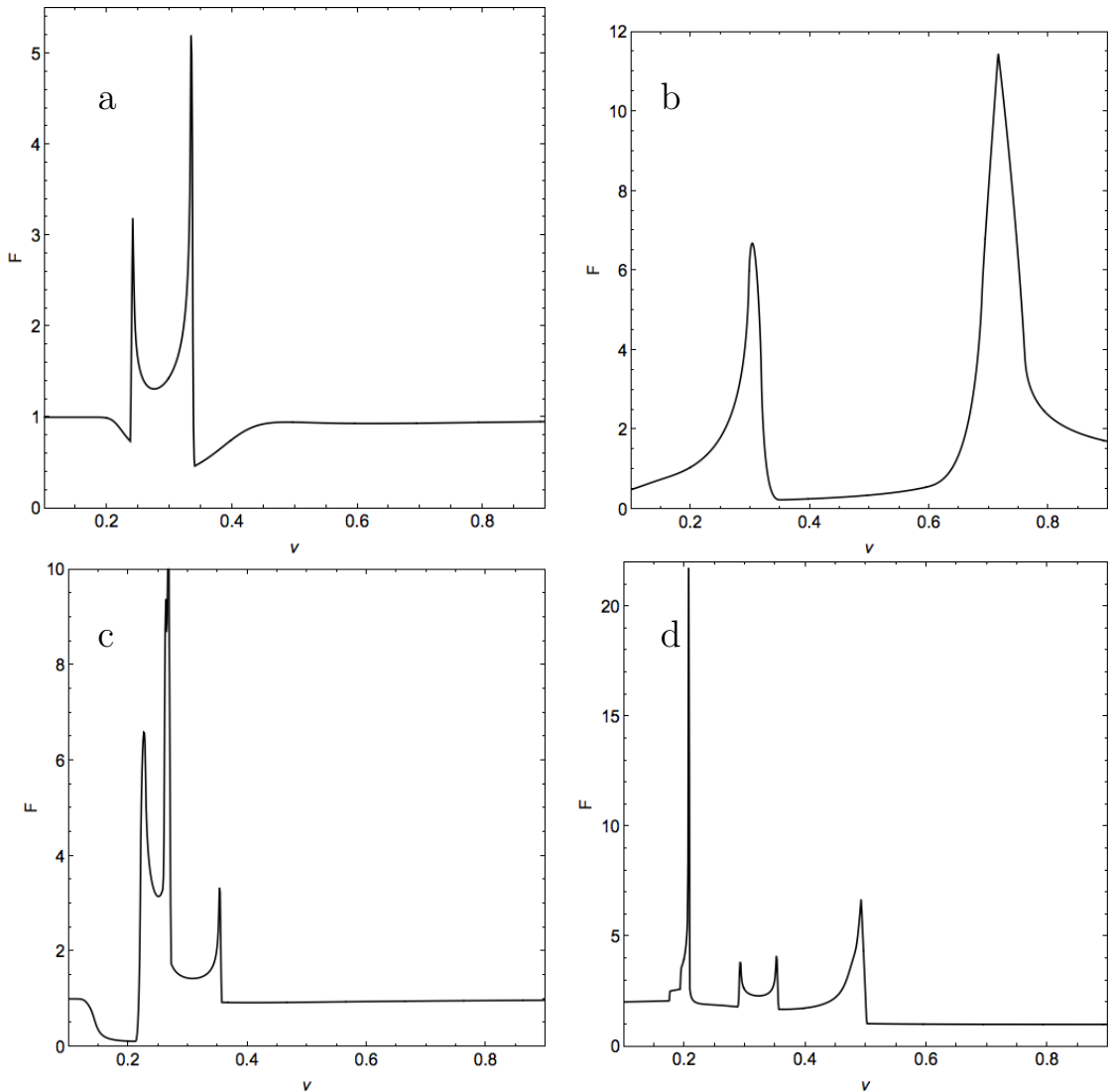


Figure 6: Individual spectra at the same positions as in Figure 2 assuming a crescent-shaped source of unit (external) radius instead of a Gaussian one (with  $\sigma = 0.3$ ). The phase of the crescent is such that its width is half the radius and it is oriented parallel to the direction of its motion in the sky, with the limb leading. The peaks at  $\nu \approx 0.7$  in panel *b* and  $\nu \approx 0.5$  in panel *d* are clearly of the ‘kinky’ type similar to those seen in the spectra, and so are the peaks at  $\nu \approx 0.25$  in panel *a* or near  $\nu \approx 0.27$ ,  $\nu \approx 0.35$  in panel *c*.

and neither it is possible for a more general source with convex isophotes and surface brightness non-decreasing towards the centre. However, negating any of the qualifiers above can potentially change the conclusion. One possibility is to consider a non-convex source and the trick does work here. For instance, the intensity density of a thin crescent of constant surface brightness might be represented as a sum of a bigger oval of positive intensity and a smaller oval of negative intensity so that they give zero in the intersection (the boundary of such a crescent is not strictly smooth but the very angles can be smoothed without affecting any of the argument below). The light curve of such a non-convex source would be given by the sum of a curve in Figure 5 and a similar curve, flipped vertically and shifted/scaled horizontally, which can be manipulated to give the appropriately oriented kink. In particular, since, according to (24), the jump in the derivative is  $\propto \sqrt{B}$  and the slope has to decrease along the way to the maximum, a terminator of a larger curvature radius than the limb would be sufficient for a job – *e.g.*, the crescent of the Moon has the shape that would produce the kink sought (cf. Ashton and Lewis 2001). Examples of such spectra are shown in Figure 6 for the same configuration as presented in Figure 2 using a Gaussian source.

There can definitely be other possibilities to produce a peak in the light curve (and, by extension of Section A, instantaneous spectrum) apart from a concave boundary. A non-constant surface brightness can do that if for no other reason that a crescent can be produced in this way. However, since a fold caustic is essentially a 1D structure, allowing variations in the surface brightness is not a huge leverage, since only the projection of the brightness onto the axis perpendicular to the fold matters; the brightness profile and the source boundary are a degenerate mix in this projection and, up to the kind of singularities allowed in either, changes in one can be emulated with changes in the other. The choice would depend on which variations required for the appropriate projection seem less contrived. A general question of what conditions are *necessary* to produce the observed kinks in the spectra requires further study.

### 2.2.1 Possible role of fold curvature

Since the shape of the light curve is given by the convolution of the fold magnification with the projection of the source surface brightness along the isomagnification lines (running, to the first approximation, parallel to the caustic), an alternative to assuming a concave shape for the source crossing a straight fold caustic is to assume that the caustic itself is curved more than the source edge and in the same direction.

This would effectively make a convex ‘hole’ in the source when lines of constant magnification are replotted straight, making the situation identical to the concave source (i.e., convex hole) on a straight fold. In other words, as the edge of the source is traced from the position of where it crosses the caustic towards their second crossing, the point should get further and further from the caustic and the magnification at this points gets lower and lower. This in turn requires that the caustic is concave when viewed from its positive side – that is the side on which sources have extra pairs of images. This does not normally happens in gravitational microlensing where caustics are convex from positive side (think astroids of the Chang-Refsdal lens!) but is not impossible if there is extended and variable component of the lensing surface density (convergence); such a reversal is even more possible in plasma lensing where there is no analogue of the Poisson equation and the convergence is not readily associated with some physical quantity.

To see that, we expand the Fermat potential near the apex of the fold (placed pretty much arbitrary along its length) as done in Section 6.2.1 of Schneider, Ehlers and Falco (1992) monograph with the following coordinate and notation conventions:

$$\phi_1 = \phi_2 = \phi_{12} = \phi_{22} = 0, \quad \phi_{11} \neq 0, \phi_{222} \neq 0, \quad \cdot_i = \partial_{\theta_i} \cdot_{\text{apex}} \quad (26)$$

where

$$\phi(\theta, \beta) = \frac{1}{2} (\beta - \theta)^2 - \psi(\theta) \quad (27)$$

and find the equation for the fold caustic:

$$Q(\beta) = Q(\beta_1, \beta_2) = Q(x, y) \equiv 2\phi_{11}\phi_{222}y - (\phi_{112}\phi_{222} - \phi_{122}^2)x^2 = 0. \quad (28)$$

We can also choose the derivative  $\phi_{222} > 0$  (if not, replace  $y \rightarrow y' = -y$  and continue in the  $(x, y')$  system), in which case the positive side of the caustic is the one above caustic (where one can take a real square root from  $Q$ ). The sense of the curvature with respect to the positive side is then specified by sign of the numerator in the coefficient of the parabola:

$$y = \frac{\phi_{112}\phi_{222} - \phi_{122}^2}{2\phi_{222}\phi_{11}^2}x^2 = \frac{x^2}{2R}, \quad (29)$$

$R$  being the curvature radius. In terms of the convergence and shear (assume there is no rotation, as is usual in thin plane lensing)

$$\phi_{ij} = \begin{pmatrix} 1 - \kappa - \gamma_c & \gamma_s \\ \gamma_s & 1 - \kappa + \gamma_c \end{pmatrix} \quad (30)$$

and hence trace  $\phi = 2(1 - \kappa)$  the curvature can be rewritten as

$$\frac{1}{2R} = -\frac{\phi_{222}^2 + \phi_{122}^2}{2\phi_{11}^2\phi_{222}} - \frac{\kappa_2}{\phi_{11}^2}. \quad (31)$$

the first terms is non-positive and thus  $1/2R$  can only be positive and thus caustic curved away from its positive (extra images) side if

$$\kappa_2 < -\frac{1}{2}\phi_{222} - \frac{\phi_{122}^2}{\phi_{222}}; \quad (32)$$

this is the condition for the reversal of the caustic convexity *vs.* image multiplicity relation with respect to that commonly encountered in microlensing where, outside point lenses,  $\kappa \equiv 0$  and hence  $\kappa_2 \equiv 0$ .

No such relation exists when  $\kappa \neq 0$  and in particular for plasma lensing where  $\kappa$  has no immediate physical interpretation other than its optics role. Therefore, it is possible that the caustic is concave when viewed from its side producing extra images, which can be further rewritten in terms of  $\kappa, \gamma_{c,s}$  as

$$\kappa_2^2 > (\gamma_{c2})^2 + (\gamma_{s2})^2 \quad \left[ \text{or } |\kappa_2| > |\gamma_2| \text{ when } \gamma = \begin{pmatrix} \gamma_c \\ \gamma_s \end{pmatrix} = \gamma \begin{pmatrix} \cos 2\chi \\ \sin 2\chi \end{pmatrix} = \gamma \hat{\mathbf{e}}_{2\chi} \text{ is treated as a vector} \right]. \quad (33)$$

However, a caustic that is highly curved relative to the curvature of the source edge necessarily affects only a small part of the source and is therefore able to produce small peaks in the spectrum but can hardly be responsible for the large-scale kink observed when PMN J1106-3647 is highly magnified.

One wonders if this difference of gravitational micro- and plasma lensing is also related to the volcano/crater puzzle (why ESEs, and in particular, achromatic ones, all seem to have the latter appearance) of Vedantham et al. (2017).

### 2.2.2 Behaviour of flux density when crossing a cusp

While a fold is a generic type of caustic in lensing and is essentially one-dimensional, there is also one other type of the caustic present in the sky – a cusp, which forms where the lens plane-to-source plane image of the point travelling along the critical curve stalls (i.e., the tangent vector to the critical curve aligns with the kernel of the deformation matrix). Cusps normally join two fold caustics forming their common end. The behaviour of the magnification on crossing to the cusp is different to approaching the fold caustic and it therefore makes sense to check whether encounter with a cusp is capable of producing a kink in the light curve (and, by extension, spectrum). The answer will turn to be negative.

The caustic curve near a cusp is a semicubic parabola (Schneider & Weiss 1992)

$$y = \pm x^{3/2}, \quad x \geq 0 \quad (34)$$

where  $x$  and  $y$  are the coordinates, respectively, along and across the symmetry axis of the cusp, and the plus or minus sign is chosen for either of the two folds joining at the cusp positioned at  $(x, y) = (0, 0)$ . The  $x$  and  $y$  are obtained by scaling the coordinates in the sky  $\xi, \eta$  by two different (in fact, of different dimension) units which depend on the derivatives of the deflection angle:

$$x = \frac{\xi}{\xi_0}, \quad y = \frac{\eta}{\eta_0} \quad \text{with} \quad \xi_0 = \frac{3(b^2 - 2ac)}{2b}, \quad \eta_0 = \frac{b^2 - 2ac}{c} \quad (35)$$

where (all non-zero)

$$a = -\frac{1}{6}\partial_\eta^3\alpha_\eta, \quad b = -\partial_\eta^2\alpha_\xi, \quad c = 1 - \partial_\xi\alpha_\xi \quad (36)$$

are the (dimensional) derivatives of the (dimensional) deflection angle  $\alpha$  with the principal axes chosen such that it is along the  $\eta$  direction that the mapping is degenerate,  $1 - \partial_\eta\alpha_\eta = 0$ .

Zakharov (1997) presents the following explicit formulae for the magnification (the book has typos at places, so the formulae would better be checked). Outside the cusp, there is a single image with the scaled magnification

$$\tilde{\mu}_O = \frac{\sqrt[3]{\sqrt{y^2 - x^3} - y} + \sqrt[3]{\sqrt{y^2 - x^3} + y}}{\sqrt{y^2 - x^3}}, \quad \text{when } x < 0 \quad \text{or} \quad x \geq 0, |y| > x^{3/2} \quad (37)$$

whereas inside there are three with

$$\tilde{\mu}_i = -\frac{2}{3}\sqrt{\frac{x}{x^3 - y^2}} \cos\left(\frac{1}{3}\arccos\sqrt{\frac{x^3 - y^2}{x^3}} + i\frac{2\pi}{3}\right), \quad i = 0, 1, 2, \quad \text{when } x > 0, |y| < x^{3/2}. \quad (38)$$

It is easy to see that  $|\tilde{\mu}_0| = |\tilde{\mu}_1 + \tilde{\mu}_2|$ ,  $\text{sgn } \tilde{\mu}_0 = -\text{sgn } \tilde{\mu}_{1,2}$  and so the sum of the absolute values of the three is

$$\tilde{\mu}_I = \sum_i |\tilde{\mu}_i| = 2|\tilde{\mu}_0| = \frac{4}{3}\sqrt{\frac{x}{x^3 - y^2}} \cos\frac{1}{3}\arccos\sqrt{\frac{x^3 - y^2}{x^3}}, \quad \text{when } x > 0, |y| < x^{3/2}, \quad (39)$$

which will be the only value of interest for us here. The actual magnification

$$\mu = \mu_0\tilde{\mu} \quad \text{with} \quad \mu_0 = \frac{1}{b^2}\left(1 - \frac{2ac}{b^2}\right)^{-1} \leftarrow \text{Zakharov (1997) suggests +1 here but that does not seem to stack up} \quad (40)$$

(similarly to  $x$  and  $y$ ,  $\tilde{\mu}$  has a curious dimension) but this does not affect qualitative behaviour of the magnification, so we will focus on the scaled quantity  $\tilde{\mu}$ .

To choose an appropriate source model (which, the model, as we argue below, is necessary), we use two observations. First, similarly to the fold case, the magnification diverges at the cusp (after all, it is a caustic) but in the 2D case we need to be more careful with the interpretation of this fact as it is the magnification in only one of the directions that diverges. For the cusp, it is the direction across the symmetry axis that is infinitely magnified and therefore resolves any source. This seems to make sense given that the cusp is ‘pointy’ with the opening angle that vanishes as the cusp point itself is approached according to (34). The appropriate model of the resolved source is therefore that of a set of (locally parallel) isophotes with some intensity density profile  $I_\nu(x)$  which make an angle  $\theta$  with the normal to the cusp axis. The angle  $\theta \neq \pi/2$  becomes irrelevant near the cusp point due to the vanishing of the opening angle though.

Second, and unlike the fold case, where highly magnified sources only appear once their source is inside the caustic, is the fact that the magnification near the cusp attains very high values even when the source is entirely outside the caustic curve. Therefore the local analysis of what happens on the contact of the source with the caustic curve is no longer sufficient.

It therefore appears that a generic source model that is able to capture the essential ingredients is that of a rectangular slab of some finite thickness  $2Y$  that has an arbitrary (finite) surface brightness profile  $I_\nu(x)$  along the cusp symmetry axis (to account for high magnification on either side of the caustic), which is independent of the perpendicular coordinate  $y$  (because this direction is arbitrarily stretched). It is also clear that we can choose the slab

to be positioned symmetrically with respect to the axis – any finite asymmetry (including the  $\theta \neq 0$  case) would be taken care of by considering fold lensing of the source, as the cusp point is but a joint of two folds. A  $y$ -dependent surface brightness profile can be synthesised as a sum of such slabs.

For such a source, we can reduce the light curve  $F_\nu(x_0)$ ,  $x_0$  marking the position of the source nominal centre, to a 1D integral w.r. to  $x$  by first integrating the scaled magnification (37,39) along the  $y$  direction explicitly:

$$F_\nu(x_0) = \int dx I_\nu(x - x_0) M_Y(x) \quad (41)$$

where (the factor of 2 is due to symmetry)

$$M_Y(x) \equiv 2\mu_0 \int_0^Y dy \tilde{\mu}(x, y) \quad (42)$$

is, at  $x < 0$ ,

$$M_Y(x < 0) = \int_0^Y dy \mu_O(x, y) = 6\mu_0 \left( \sqrt[3]{\sqrt{Y^2 - x^3} + Y} - \sqrt[3]{\sqrt{Y^2 - x^3} - Y} \right) \quad (43)$$

whereas at  $x > 0$

$$M_Y(x > 0) = 2\mu_0 \left[ \int_0^{x^{3/2}} dy \mu_I(x, y) + \int_{x^{3/2}}^Y dy \mu_O(x, y) \right] = 2\mu_0 \left[ 3 \left( \sqrt[3]{Y + \sqrt{Y^2 - x^3}} + \sqrt[3]{Y - \sqrt{Y^2 - x^3}} \right) - 4\sqrt{x} \right] \quad (44)$$

where we used that  $x^{3/2} < Y$  at sufficiently low  $x$ ; further away, at  $x > Y^{2/3}$  one instead has

$$M_Y(x > Y^{2/3}) = 2\mu_0 \int_0^Y \mu_I(x, y) = 8\mu_0 \sqrt{x} \sin \frac{1}{3} \arccos \sqrt{1 - \frac{Y^2}{x^3}}. \quad (45)$$

The resulting  $M_Y(x)$  is shown in Figure 7 for a selection of widths  $Y$ . They are all non-smooth at  $x = 0$  as the derivative diverges on the positive side due to the  $\sqrt{x}$  term while remaining finite to the left of the origin:

$$M'_Y(x \rightarrow 0 - 0) \rightarrow 3\mu_0 2^{2/3} Y^{5/3} \quad \text{but} \quad M'_Y(x \rightarrow 0 + 0) \rightarrow -\infty. \quad (46)$$

However, the kernels  $M_Y(x)$  remain finite and continuous across this irregularity

$$M_Y(x \rightarrow 0 \pm 0) \rightarrow 6\mu_0 \sqrt[3]{2Y} \quad (47)$$

and therefore result in smooth functions of  $x$  when convolved with a regular source profile in (41); the worst case scenario for a finite  $I_\nu(x)$  would be finite discontinuities and these integrate to  $\propto x^{3/2}$  terms when convolved with the  $x \rightarrow 0$  irregularity in  $M_Y(x)$  – resulting in a smooth  $F_\nu(x)$ . The same argument applies to the irregularity at  $x = Y^{2/3}$  but here the non-smoothness is even milder ( $M'_Y(x)$  remains finite of both sides) and  $Y$ -dependent.

In conclusion, a source with finite brightness temperature undergoing lensing on a cusp, cannot display a discontinuity in the derivative its light curve or instantaneous spectrum, they have to be smooth. One caveat is that although, as shown above, a finite brightness source regularises any potential kink due to transition through a cusp into a smooth light curve or instantaneous spectrum, the scale of this smoothing might be below the resolution in the data. In this case, the effective magnification is  $M_Y(x)/Y$  and one expects to see data akin to the curves shown in Figure 7. The apparent non-smoothness in the data can then be used to infer an upper limit on the source dimension along the cusp axis and the dimension across the axis can be estimated from the peak brightness via (47), up to the value of  $\mu_0$ . If the position of the second kink and the magnification scale can be estimated, this provides means to solve for the parameters of rescaling (35, 40), in the units of source angular dimensions. Note, however, that the essentially point-like nature of the source in the  $x$  direction implies that the light curve should be very close to the prescription of  $M_Y(x)/Y$ . In particular, the one side of the kink in the light curve should be vertical at the same data resolution, with a divergent derivative; on the same side, the second derivative has to be positive. Therefore, a non-vertical kink – that is, a finite jump in the derivative, remains a unique signature of a source with a smooth sharp boundary crossing a fold caustic, as derived in the previous section.

One final note is that unlike gravitational lensing, where folds and cusps are the only two generic types of caustics, higher order caustics (beak-to-beak, lips and swallowtails) are possible in plasma lensing as a result of the deflection angle dependence on the wavelength. However, these only form at special points in all three variables (wavelength and position in the sky) and are therefore unlikely to be observationally sampled; they are to be presented studied separately.

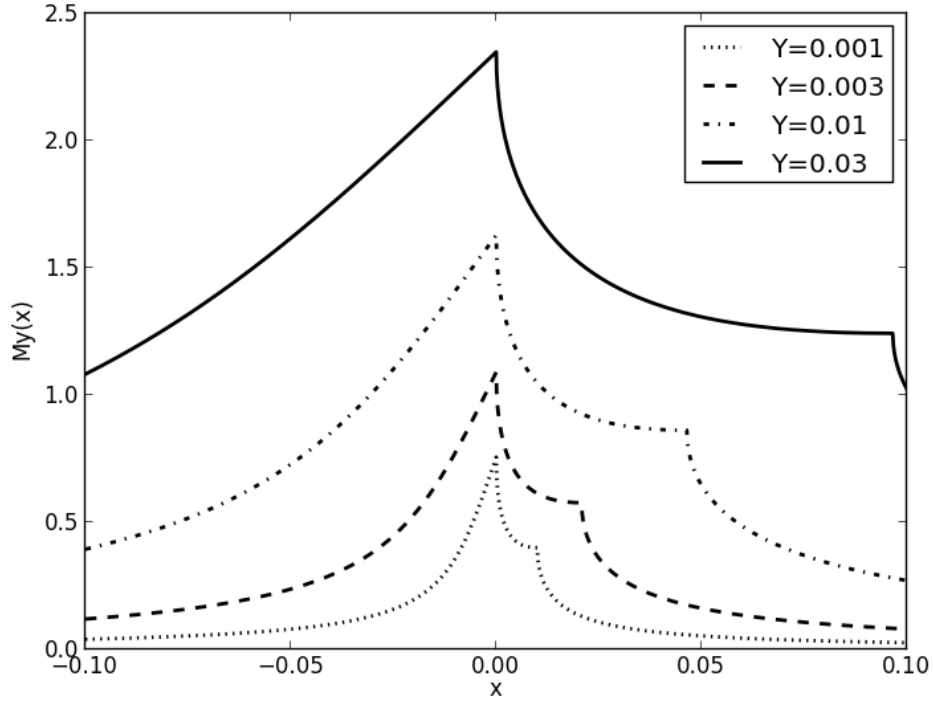


Figure 7: One-dimensional integral (42) of the magnification along the column orthogonal to the cusp axis,  $M_Y(x)$  as a function of the position with respect to the cusp ( $x > 0$  is inside the caustic curve) and the height of the column  $Y$ .

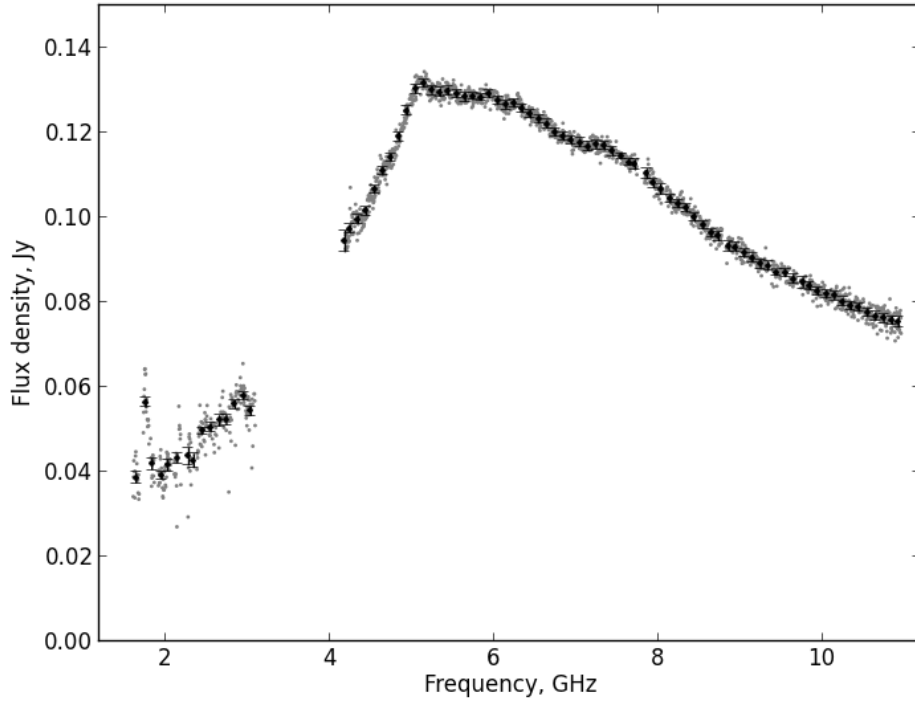


Figure 8: The quasi-simultaneous spectrum of PMN J1106-3647 obtained on MJD 57087. The original data from 72 sub-epochs (24 for each configuration of the correlator) with 10 s long exposures are shown as grey points and the black points are averages of all data points in 0.1 GHz wide bins. The error bars shown are five times the estimate of the uncertainty of averages.

## A Crossing caustic in Dynamic spectrum

To model effects of the caustic crossing in a single spectrum we just allow all variables specifying the shape and position of the source and properties of the cusp (*e.g.*, in (16) and its analogues) to be functions of frequency. As we expect all intrinsic properties to behave well with frequency, the most conspicuous manifestation of the caustic crossing should come from  $f$  and roughly mirror the shapes in Figure 4, multiplied by, to the first order, a linear function of frequency  $F_0/\lambda\sqrt{\sigma/\rho}$  and sitting on top of a linear function describing the spectral variation in images other than the caustic pair. The argument of the shape function  $f$  is, at the vicinity of the caustic,

$$\begin{aligned} \frac{\beta_c - \beta_0}{\sigma} &\simeq \frac{\beta_c(\nu_0) + \partial_\nu \beta_c(\nu_0)(\nu - \nu_0) - \beta_0(\nu_0) - 2\lambda^2(\nu_0)\alpha[\theta(\nu_0)](\nu - \nu_0)/\nu_0}{\sigma(\nu_0) + \partial_\nu \sigma(\nu_0)(\nu - \nu_0)} + \mathcal{O}(\nu - \nu_0)^2 \\ &\simeq \frac{\partial_\nu \beta_c(\nu_0) - 2\lambda^2(\nu_0)\alpha[\theta(\nu_0)]/\nu_0}{\sigma(\nu_0)} (\nu - \nu_0) + \mathcal{O}(\nu - \nu_0)^2, \end{aligned} \quad (48)$$

where we used (7), also returning to its notation, denoted the frequency where the spectrum of interest crosses the caustic as  $\nu_0$  and took into account that  $\beta_c - \beta_0 = 0$  at  $\nu_0$  by definition.

In other words, barring significant core shifts (with which the deflection angle is of course degenerate), the fractional width of the caustic crossing on frequency axis (at some given level corresponding to a certain range  $\Delta x$  in the shape function  $f(x)$  argument) is (twice) the source size in units of the deflection angle at the crossing frequency

$$\frac{\sigma(\nu_0)}{\lambda(\nu_0)^2\alpha[\theta(\nu_0)]} = \frac{2\Delta\nu}{\nu_0\Delta x}, \quad (\partial_\nu \beta_c = 0) \quad (49)$$

Meanwhile, the amplitude of the caustic signal can be used to find  $\sigma$  in combination with the second derivative of the deflection angle at the same point

$$\frac{\sigma\lambda^2}{\rho} = \sigma\lambda^2|\alpha''| = \left(\frac{F_0 f_{\max}}{F_{\max}}\right)^2. \quad (50)$$